UDC 669.2/.8.017
https://doi.org/10.17073/0021-3438-2023-4-35-47

Research article
Научная статья

# Improvement of selective laser melting regimes for the fabrication of Ti–6Al–4V porous structures for medical applications

**V.A. Sheremetyev[1], V.D. Lezin[1], M.V. Kozik[1], S.A. Molchanov[2]**

[1] **National University of Science and Technology "MISIS"**
4 bld. 1 Leninskiy Prosp., Moscow 119049, Russia

[2] **LLC "Conmet"**
24/1 Onezhskaya Str., Moscow 125413, Russia

✉ Vadim A. Sheremetyev (vadim.sheremetyev@gmail.com)

**Abstract:** This article describes approaches to the optimization of regimes of selective laser melting (SLM) used in the fabrication of porous materials from medical grade Ti–6Al–4V alloy with thin structural elements and a low level of defect porosity. Improved fusion of thin elements based on SLM regimes is achieved due to a significant decrease in the distance between laser passes (from 0.11 to 0.04–0.05 mm). Moreover, the balance between the laser energy density and building rate is compensated by changing the laser speed and laser power. The results of the study of defect porosity and hardness of samples fabricated according to experimental SLM regimes allowed three promising sets of parameters to be defined. One was selected for studying mechanical properties in comparison with the reference SLM regime. In the aims of this study, the samples were developed and fabricated using the structures of rhombic dodecahedron and Voronoi types with a porosity of 70–75 %. The decrease in defect porosity was established at ≈1.8 % to 0.6 %, depending on the SLM regime. This promotes a significant increase in strength properties of the material, including an increase in the yield strength of rhombic dodecahedron from 76 to 132 MPa and the Voronoi structure from 66 to 86 MPa. The low Young module (1–2 GPa) remains, corresponding to the rigidity level of spongy bone tissue.

**Keywords:** selective laser melting, titanium alloys, porous structures, microstructure, porosity, mechanical properties.

**Acknowledgements:** This work was supported by Grant No. 22-79-10299 of the Russian Science Foundation, https://rscf.ru/project/22-79-10299/

**For citation:** Sheremetyev V.A., Lezin V.D., Kozik M.V., Molchanov S.A. Improvement of selective laser melting regimes for the fabrication of Ti–6Al–4V porous structures for medical applications. *Izvestiya. Non-Ferrous Metallurgy.* 2023;29(4):35–47.
https://doi.org/10.17073/0021-3438-2023-4-35-47

# Совершенствование режима селективного лазерного плавления для изготовления пористых структур из сплава Ti–6Al–4V медицинского назначения

**В.А. Шереметьев[1], В.Д. Лезин[1], М.В. Козик[1], С.А. Молчанов[2]**

[1] **Национальный исследовательский технологический университет «МИСИС»**
Россия, 119049, г. Москва, Ленинский пр-т, 4, стр. 1

[2] **ООО «Конмет»**
Россия, 125413, г. Москва, ул. Онежская, 24/1

✉ Вадим Алексеевич Шереметьев (vadim.sheremetyev@gmail.com)

**Аннотация:** Разработаны подходы к оптимизации режима селективного лазерного плавления (СЛП) для получения пористых материалов из сплава Ti–6Al–4V медицинского назначения с тонкими конструкционными элементами и низким уровнем дефектной

© 2023 г. V.A. Sheremetyev, V.D. Lezin, M.V. Kozik, S.A. Molchanov

пористости. Улучшенное проплавление тонких элементов с применением разработанных экспериментальных режимов СЛП достигается за счет значительного снижения расстояния между проходами лазера (с 0,11 до 0,04–0,05 мм), а баланс между плотностью энергии лазера и скоростью построения скомпенсирован путем изменения скорости пробега и мощности лазера. Результаты изучения дефектной пористости и твердости образцов, изготовленных по экспериментальным режимам СЛП, позволили установить 3 наиболее перспективных набора параметров, один из которых выбран для исследования механических свойств в сравнении со стандартным режимом СЛП. Для этого исследования разработаны и изготовлены образцы на основе структур типа ромбического додекаэдра и полиэдра Вороного пористостью 70–75 %. Установлено, что снижение уровня дефектной пористости с ≈1,8 % до 0,6 %, обеспеченное применением разработанного режима СЛП, способствует значительному повышению прочностных характеристик материала. Увеличение условного предела текучести ромбического додекаэдра с 76 до 132 МПа и Вороного с 66 до 86 МПа. При этом сохраняется низкий модуль Юнга (1–2 ГПа), соответствующий уровню жесткости губчатой костной ткани.

**Ключевые слова:** селективное лазерное плавление, титановые сплавы, пористые структуры, микроструктура, пористость, механические свойства.

**Благодарности:** Работа выполнена за счет гранта Российского научного фонда № 22-79-10299, https://rscf.ru/project/22-79-10299/

**Для цитирования**: Шереметьев В.А., Лезин В.Д., Козик М.В., Молчанов С.А. Совершенствование режима селективного лазерного плавления для изготовления пористых структур из сплава Ti–6Al–4V медицинского назначения. *Известия вузов. Цветная металлургия.* 2023;29(4):35–47. https://doi.org/10.17073/0021-3438-2023-4-35-47

## Introduction

Selective laser melting (SLM), consisting of layer-by-layer melting of a metal powder under the impact of a moving laser beam, has become widespread in the production of medical implants and tools. This is due to the rapid transition to manufacturing, greater freedom in product design, and the high accuracy of their geometry. Standardized medical alloys Ti—6Al—4V, Ti—6Al—7Nb are widely employed [1; 2] in the manufacture of implants using the SLM method. This also includes as Ti—Ni, Ti—Zr—Nb shape memory alloys for medical purposes [3; 4].

In the medical industry, the advantage of SLM over traditional manufacturing methods, in addition to manufacturing individual implants, also lies in the possibility of obtaining porous structures with a given geometry and cell size. The use of porous structures arises from the necessity to simulate the structure of bone tissue and its properties (Young's modulus, compressive strength, biological compatibility, tendency to bone tissue ingrowth) [5]. The ingrowth of bone tissue into the implant is one of the most important properties, and provides a reliable mechanical connection with the bone [6; 7]. This property is determined by such macrostructural parameters as porosity (the proportion of voids in the total volume of the product), dimensions, geometric shape and pore distribution.

In the last decade, the development of new bone structures, and optimization of the geometry of existing porous structures, for bone implants has been the subject of numerous works [8—11]. Two approaches to the creation of such structures can be identified:

— non-parametric design, when the structure is created on the basis of the geometry of a single element;

— parametric design, based in an algorithm with input data in the form of porous structure parameters (porosity, pore size). The structure is generated with some element of randomness, based on mathematical expressions [5].

Of the existing variety of types of porous structures, two were selected for study: a rhombic dodecahedron (*D*, nonparametric design); and Voronoi polyhedra (*V*, parametric design). Materials based on a *D*-type cell are distinguished by the homogeneity of the macrostructure and the high strength properties in all directions [12]. Structure *V* is less homogeneous, but similar in morphology to real bone tissue [13]. It is formed by creating a grid structure based on connecting random discrete points with struts, in accordance with a certain algorithm [14].

Increase in the functional and mechanical properties of materials obtained by the SLM method is associated with the minimization of internal material defects in the form of pores in the struts. Defect porosity is formed due to insufficient or excessive energy density, determining the conditions for powder melting [15]. In order to eliminate defective porosity, it is necessary to correctly select the SLM parameters [4]. When applied to porous structures, where the thickness of internal structural elements ("struts") is 200—300 μm, the problem of defective porosity, as well as geometry accuracy, is of particular importance from the point of view of increasing the strength characteristics of products

[16]. The solution to this problem can achieved by correcting the laser trajectory and reducing the distance between its passes. This in turn requires the other SLM parameters to be changed, in order to ensure optimal energy density.

This study focuses on improving the SLM regime for fabricating porous structures of the *D* and *V* types with thin structural elements and a low level of defect porosity from a Ti—6Al—4V alloy (ASTM F3001) for medical purposes.

## Experimental

The initial material employed in this research was Ti—6Al—4V alloy powder (AP&C a GE Additive Company, Canada). According to the ASTM B822 specification, particle size distribution is as follows: $d10$ = = 23 μm, $d50$ = 35 μm, $d90$ = 47 μm. Fluidity according to ASTM B213 and bulk density according to ASTM B213 were 25 s/50 g and 2.55 g/cm$^3$, respectively. Experimental samples were fabricated using a TRUPRINT1000 laser setup (TRUMPF Gruppe, Germany) equipped with an ytterbium laser with a power of $P_L$ = 175 W, spot diameter of 30 μm, and a maximum laser speed of $v \le 3000$ mm/s. In order to control the SLM regimes, the thickness of the powder layer ($t$) and the scanning step ($h$) can be varied. This can be determined by the distance between the laser passes in one layer.

A standard regime (hereinafter *T*) is used, according to the recommendation by the manufacturer, TRUMPF (Germany), for the manufacture of products from this powder. This includes two sets of parameters: for building the main (internal) and contour (external) parts of the product (Table 1).

The main regime is formed by "hatching" with a certain step to build the bulk of the product and must meet the requirements of optimal penetration of the powder layer, in order to ensure low defective porosity ($p_d$). The tracing regime has one pass along the contour of the object in each layer and serves to ensure the required surface quality of the product. In order to optimize the SLM parameters, it is customary to use the following characteristics: energy density ($E$) and build rate ($BR$), calculated by the following equations [17]:

$$E = \frac{P_L}{vht}, \quad (1)$$

$$BR = vht. \quad (2)$$

After fabrication, all samples were subjected to heat treatment in a vacuum furnace according to the standard regime: annealing at 1010 °C (45 min) followed by cooling in the furnace. After heat treatment, the samples were cut from the platform using the EDM method.

In order to assess defect porosity by metallographic analysis, thin sections were prepared by multi-stage grinding and polishing in two stages:

— mechanical grinding on abrasive SiC-paper with particle size from P320 to 4000;

— polishing using a suspension based on silicon oxide with a particle size of 0.05 μm.

Thin polished sections were analyzed using a VERSAMET-2 metallographic microscope (UNITRON, Japan) at 50× magnification. The resulting photographs of the microstructure were processed using ImageJ software (Wayne Rasband (NIH), USA). The ratio of the area of dark segments (pores) to the entire area of the micrograph was used to determine the defect porosity of the segment.

The porosity of the experimental samples ($p$) was determined by weighing the density of the Ti—6Al—4V compact alloy. This was calculated by the following equation:

$$p = \left(1 - \frac{\rho_{por}}{\rho_{mon}}\right) \cdot 100\ \%, \quad (3)$$

where $\rho_{por}$ is the density of porous sample, and $\rho_{mon}$ = = 4.47 g/cm$^3$ is the density of Ti—6Al—4V solid alloy.

The density of porous samples was estimated by weighing them and calculating according to the following equation:

$$\rho_{por} = \frac{m_{por}}{V_{ctl}} \cdot 100\ \%, \quad (4)$$

where $m_{por}$ is the weight of sample, g; $V_{stl}$ is the model volume, cm$^3$.

Table 1. **Parameters of SLM regimes recommended by the manufacturer**

Таблица 1. Параметры режимов СЛП, рекомендованные производителем

| Regime | $P_L$, W | $t$, mm | $h$, mm | $v$, mm/s | $E$, J/mm$^2$ | $BR$, cm$^3$/h |
|---|---|---|---|---|---|---|
| Main | 155 | 0.02 | 0.11 | 1200 | 58.71 | 9.50 |
| Tracing | 75 | 0.02 | – | 1000 | – | – |

*X*-ray diffraction analysis was carried out using a D8 ADVANCE X-ray diffractometer (Bruker, Germany) at room temperature in Cu$K_\alpha$ radiation in the range of 2θ = 30°÷80°. The microstructure of the samples was studied using a VEGA LMH scanning electron microscope (TESCAN, Czech Republic) equipped with an electron backscatter diffraction (EBSD) device.

The Vickers hardness of the samples was determined using a Metkon Metallography hardness tester (Metkon, Turkey), performing at least 5 measurements for each sample at a load of 1 kg and a holding time of 10 s.

The mechanical properties of the samples of porous structures in the form of cylinders with a diameter of 14.0—14.5 mm and a height of 7.0—7.5 mm were evaluated by uniaxial compression tests. The tests were carried out on an Instron 5966 testing machine (Instron — Division of ITW Ltd., USA) at a strain rate of 2 mm/min until a relative strain of 50 % was reached. The values of Young's modulus ($E$), yield strength ($\sigma_{0,2}$) and ultimate strength ($\sigma_u$) were determined according to the deformation curves obtained. For testing purposes, 3 samples were used for each experimental point. The calculated values of mechanical properties were averaged. The measurement error was determined as the standard deviation

## Results and discussion

### Selection of parameters of porous structures and development of models

As described above, two types of porous structures, *D* and *V*, were selected for study in this work. Their geometric characteristics were selected based on the analysis of the publications, as well as the requirements for porous structures to ensure osseointegration. The technological possibilities of manufacturing [8] were also taken into account.

The selection of the optimal pore size is limited by a very wide range $D$ = 0.1÷1.0 mm [18]. Pore sizes $D$ = 0.1÷0.2 mm are sufficient to accommodate individual osteo-like cells (osteoblasts). $D$ = 0.2÷0.6 mm allow colonization of osteoblasts, while an increase in pore size above 0.6 mm contributes to vascularization, the formation of new blood vessels and bone tissue [8, 10].

The higher the porosity of the material, the greater the internal free volume for the bone tissue. However, according to [19, 20], at porosity values $p$ > 75 %, the strength parameters of porous structures degrade significantly to levels below those of bone tissue.

The thickness of thin internal structural elements ("struts") largely determines the porosity of the final structure, and is limited by the capabilities of SLM. According to [8; 9], the minimum size of such elements to ensure high accuracy is 0.20—0.25 mm. Considering these requirements and using the Materialize 3-matic software (Belgium), models of porous structures and cylindrical samples were created for subsequent fabrication and evaluation of their mechanical properties (see Fig. 1). In order to determine the parameters of the resulting porous structures (porosity ($p$), pore size ($D$), and strut thickness ($h$)) CAD models were analyzed using VGStudio MAX 3.1 software (Germany). The parameters of the developed porous structures are summarized in Table. 2.

The struts of the structure with a *D* type cell have the same thickness. Their location at an angle of 45° relative to the axes ensures the uniformity of mechanical properties in all directions (see Fig. 1). In a structure element of *V* type of a similar size, struts with a variable thickness are observed, although their arrangement looks chaotic. Due to randomization during the generation of such a structure, the pores also have different sizes.

### Development of experimental SLM regimes

Table. 1 shows a laser scanning step of 0.11 mm. This is too large for building thin structural elements, since it is comparable to the strut thickness (0.25 μm) (see Fig. 2). Therefore, in order to build the porous structures, the main SLM regimes with a scanning step of 0.04 and 0.05 mm were selected. Fig. 2 shows that a laser movement strategy enables the main regime to be applied more efficiently when building small-sized elements by increasing the number of laser passes inside the struts.

While developing the experimental SLM regimes, the values of the energy density and the building rate of the regime by the manufacturer were taken as a guide-

Table 2. **Parameters of the developed models of porous structures**

Таблица 2. Параметры разработанных моделей пористых структур

| Structure type | Strut thickness, mm | Pores size, mm | Porosity, % |
|---|---|---|---|
| *D* | ~0.26 | 0.4–0.5 | ~75.3 |
| *V* | 0.20–0.25 | 0.2–0.8 | ~75.5 |

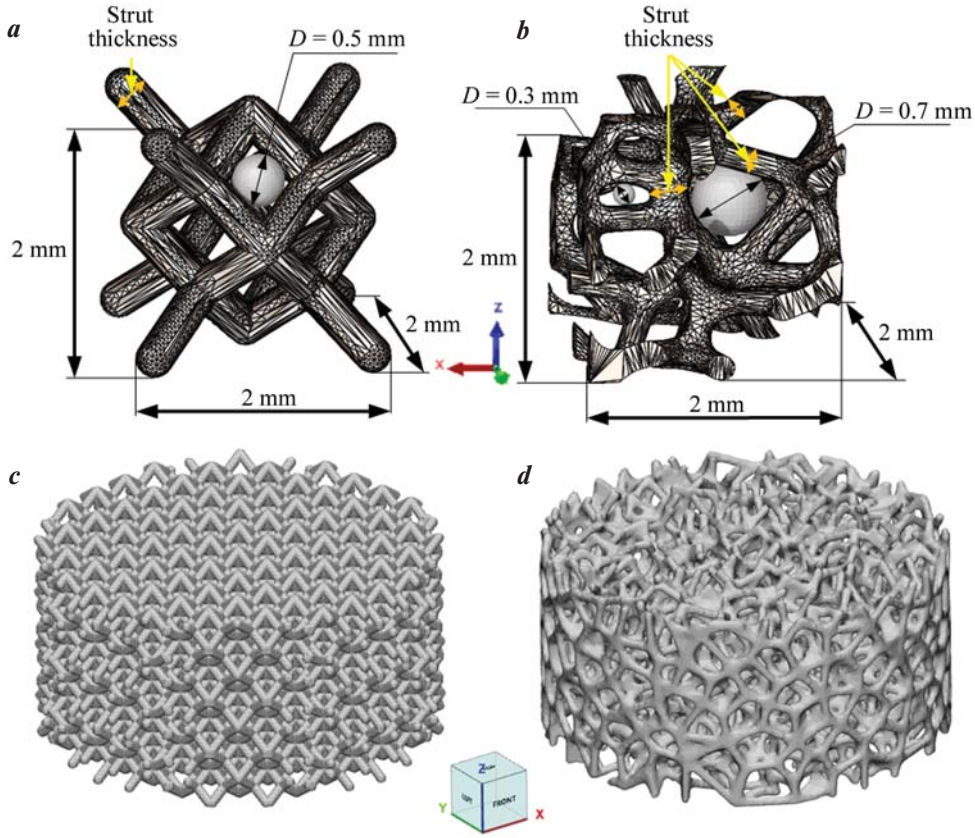


**Fig. 1.** Elementary cell of *D* type structure (***a***) and cell of *V* type structure of similar size (***b***), models of experimental samples of porous structures *D* (***c***) and *V* (***d***) for mechanical tests

**Рис. 1.** Элементарная ячейка структуры типа *Д* (***a***) и элемент структуры *В* аналогичного размера (***b***), а также модели экспериментальных образцов пористых структур *Д* (***c***) и *В* (***d***) для механических испытаний

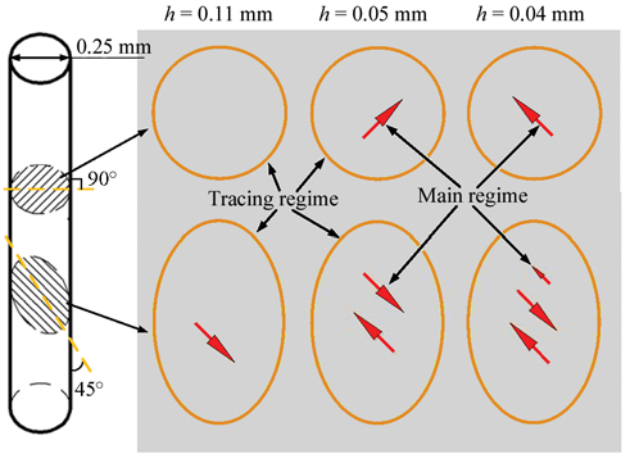


**Fig. 2.** Schematic view of laser trajectories when plotting a cylinder with a diameter of 0.25 mm in two different sections using SLM regimes with a scanning step of 0.11, 0.05 and 0.04 mm

**Рис. 2.** Схемы траекторий движения лазера при построении цилиндра диаметром 0,25 мм в двух разных сечениях при использовании режимов с шагом сканирования 0,11, 0,05 и 0,04 мм

line. These conditions enabled products with a low level of defect porosity (less than 0.5 %) to be obtained. Moreover, based on the data of [17], a conditional region was marked on the graph of energy density dependence on building rate. This corresponds to a combination of SLM parameters to obtain products with a minimum number of internal defects (Fig. 3). An additional limitation in the selection of SLM parameters is the limiting speed of building products (vertical lines in Fig. 3), determined by the scanning step (0.04 and 0.05 mm) and the limiting scanning speed. As a result of the selection of SLM parameters, 9 experimental modes were developed (Table 3). These are shown on the map of their dependence on the energy density and building rate (see Fig. 3).

## Study of defect porosity and hardness of samples fabricated according to experimental SLM regimes

Using the regimes developed, 9 samples were fabricated in the form of a cube with the size of 3×3×3 mm.

Table 3. **Parameters of the developed experimental SLM regimes and standard regime *T***

Таблица 3. Параметры разработанных экспериментальных режимов СЛП и стандартного режима *T*

| SLM regime | $P_L$, W | *h*, mm | *v*, mm/s | *E*, J/mm$^2$ | *BR*, cm$^3$/h |
|---|---|---|---|---|---|
| *1* | 136 | 0.04 | 2900 | 58.62 | 8.35 |
| *2* | 143 | 0.04 | 2600 | 68.75 | 7.49 |
| *3* | 160 | 0.04 | 2900 | 68.97 | 8.35 |
| *4* | 140 | 0.05 | 2860 | 48.95 | 10.30 |
| *5* | 155 | 0.05 | 2630 | 58.94 | 9.47 |
| *6* | 155 | 0.05 | 2250 | 68.89 | 8.10 |
| *7* | 175 | 0.05 | 2630 | 66.54 | 9.47 |
| *8* | 135 | 0.05 | 2630 | 51.33 | 9.47 |
| *9* | 167 | 0.05 | 2860 | 58.39 | 10.3 |
| *T* | 155 | 0.11 | 1200 | 58.71 | 9.50 |

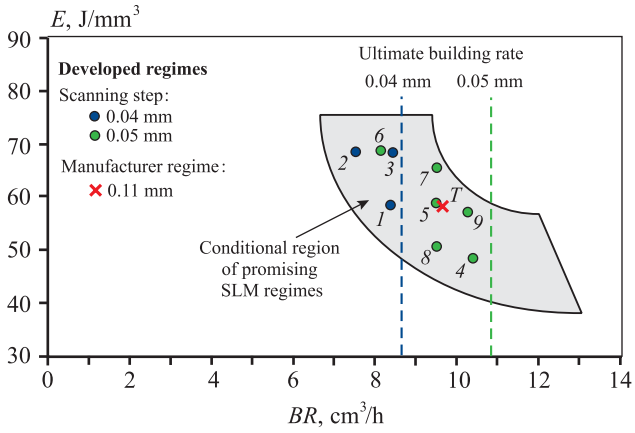


**Fig. 3.** Distribution map of experimental (***1–9***) and standard (*T*) SLM regimes as a function of energy density and building rate

The conditional area of promising SLM regimes is highlighted in gray

**Рис. 3.** Карта распределения экспериментальных (т. ***1–9***) и стандартного (*T*) режимов СЛП в зависимости от плотности энергии и скорости построения

Условная область перспективных режимов СЛП выделена серым

Their external view is illustrated in Fig. 4. The e sample obtained according to regime *2* is visually distinguished by the presence of defects on the surface. This regime with the minimum *BR* is the extreme one in the plot of energy density and building rate (see Fig. 3).

Fig 5 shows measurements of defect porosity ($p_d$) and hardness of the samples obtained using the experimental regimes and under standard conditions (*T*). A high level of $p_d$ values correlates with a large error in measuring the hardness *HV*. This can be explained by the indenter entering in the immediate vicinity of the pores. The material produced according to regimes *1*, *5*, and *7* has the lowest defect porosity and high hardness comparable to the level of these characteristics for the alloy produced according to regime *T*. These regimes correspond to a rather narrow range of parameters ($E$ = 58.6÷66.5 J/mm$^2$, $BR$ = = 8.4÷9.5 cm$^3$/h). Taking into account the measurement results, as well as the minimum scanning step (0.04 mm), regime *1* was selected for further research and fabrication of porous structures in comparison with standard conditions *T*.

## Study of phase composition and microstructure

Fig. 6 shows the results of the *X*-ray diffraction analysis of the alloy fabricated according to regimes *T* and *1* before and after heat treatment (HT). In all cases, the alloy is in the single-phase state of the low-temperature hexagonal close-packed (HCP) α-phase. No clear *X*-ray lines of the high-temperature BCC β-phase were found in the *X*-ray diffraction patterns.

The microstructure of the alloy after SLM was studied in two regimes with subsequent heat treatment. It was performed using electron backscatter diffraction in a plane parallel to the building plane. Fig. 7 shows

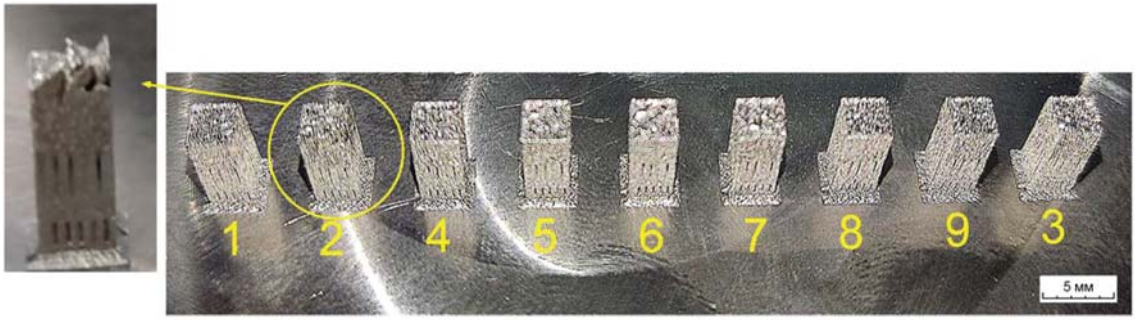


**Fig. 4.** External view of samples obtained according to the experimental SLM regimes ***1–9*** (see Table 3), with supports on the platform

**Рис. 4.** Внешний вид образцов, полученных по экспериментальным режимам СПЛ ***1–9*** (см. табл. 3), с поддержками на платформе

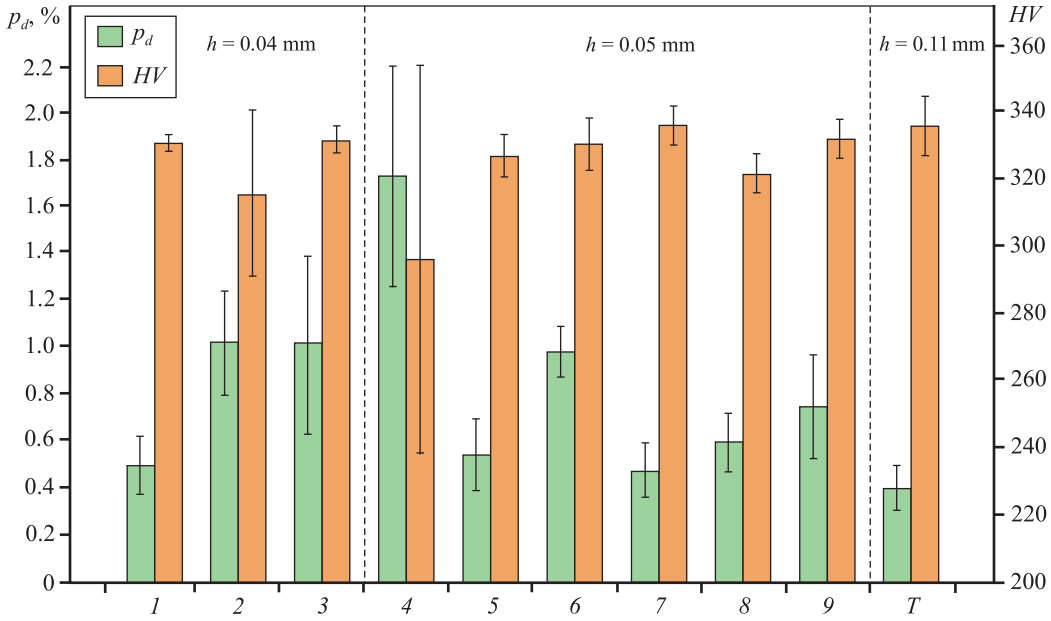


**Fig. 5.** Defect porosity and hardness of samples obtained by experimental regimes ***1–9***, compared with the standard regime *T*

**Рис. 5.** Дефектная пористость и твердость образцов, полученных по экспериментальным режимам ***1–9***, в сопоставлении со стандартным режимом *T*

that changing the regime does not lead to a change in the structural state of the material. The microstructure is predominantly represented by α-phase plates 1—5 μm thick formed as a result of β → α-transformation during cooling after annealing. The contours of the packets of α-phase plates are the former (inherited) grain boundaries of the high-temperature β-phase, within which the packets were formed.

The phase state and microstructure of the alloy fully correspond to those obtained using the standard SLM mode after HT in the earlier study of this alloy [20].

## Study of the macrostructure and mechanical properties of porous structures

Fig. 8 shows the macrostructure of porous samples obtained according to regime *1*. A considerable quantity of fused granules of powder material is observed on the inner surface. In the lower part of the samples, these particles are much more numerous. This can be explained by the features of the SLM process and is consistent with the observations of other researchers [21]. Granules on the surface create stress concentrators, contribute to

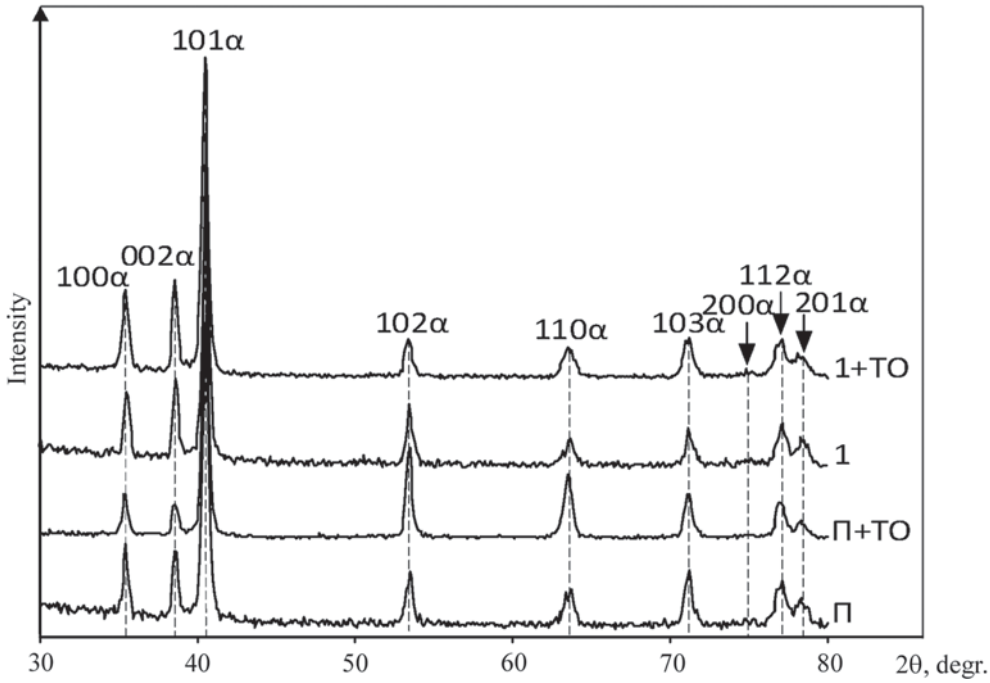


**Fig. 6.** *X*-ray diffraction patterns of samples obtained by regimes *T* and *1*, before and after heat treatment

**Рис. 6.** Рентгеновские дифрактограммы образцов, полученных по режимам *T* и *1*, до и после термообработки

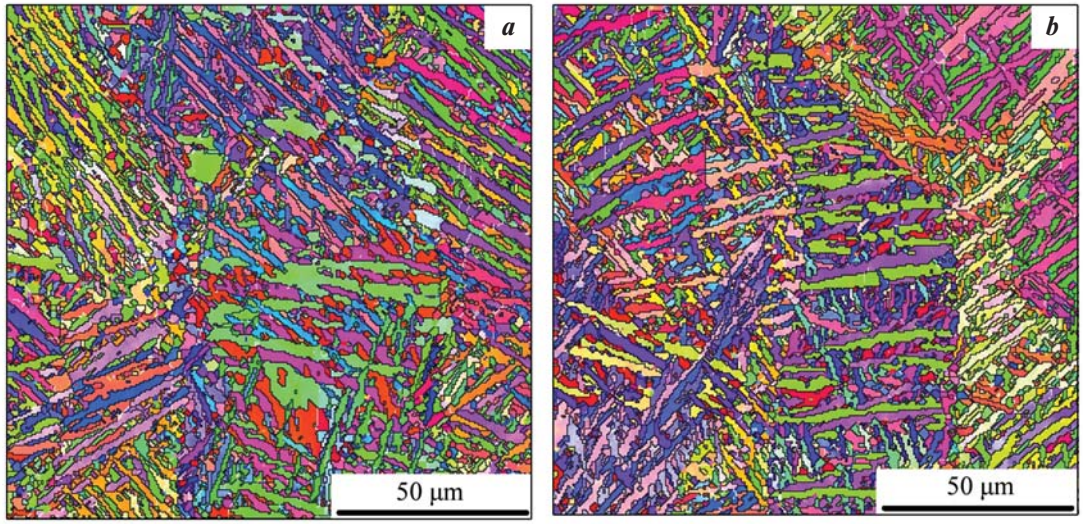


**Fig. 7.** Microstructure of samples obtained by regimes *T* (***a***) and *1* (***b***), after heat treatment

**Рис. 7.** Микроструктура образцов, полученных по режимам *T* (***a***) и *1* (***b***), после термообработки

the initiation of fatigue cracks and reduce the fatigue strength of the material, thus they need to be removed [21]. In addition, their presence makes it difficult to quantify the accuracy of the geometry of thin structural elements.

Fig. 9 shows quantitative assessment of defect porosity and geometry was carried out by analyzing images in several sections of the sample obtained using light electron microscopy. Qualitative assessment of the images showed a difference in the level of defect porosity between the samples made according to regimes *T* and *1*.

It was established as a result of the quantitative analysis of defective porosity that for structures obtained

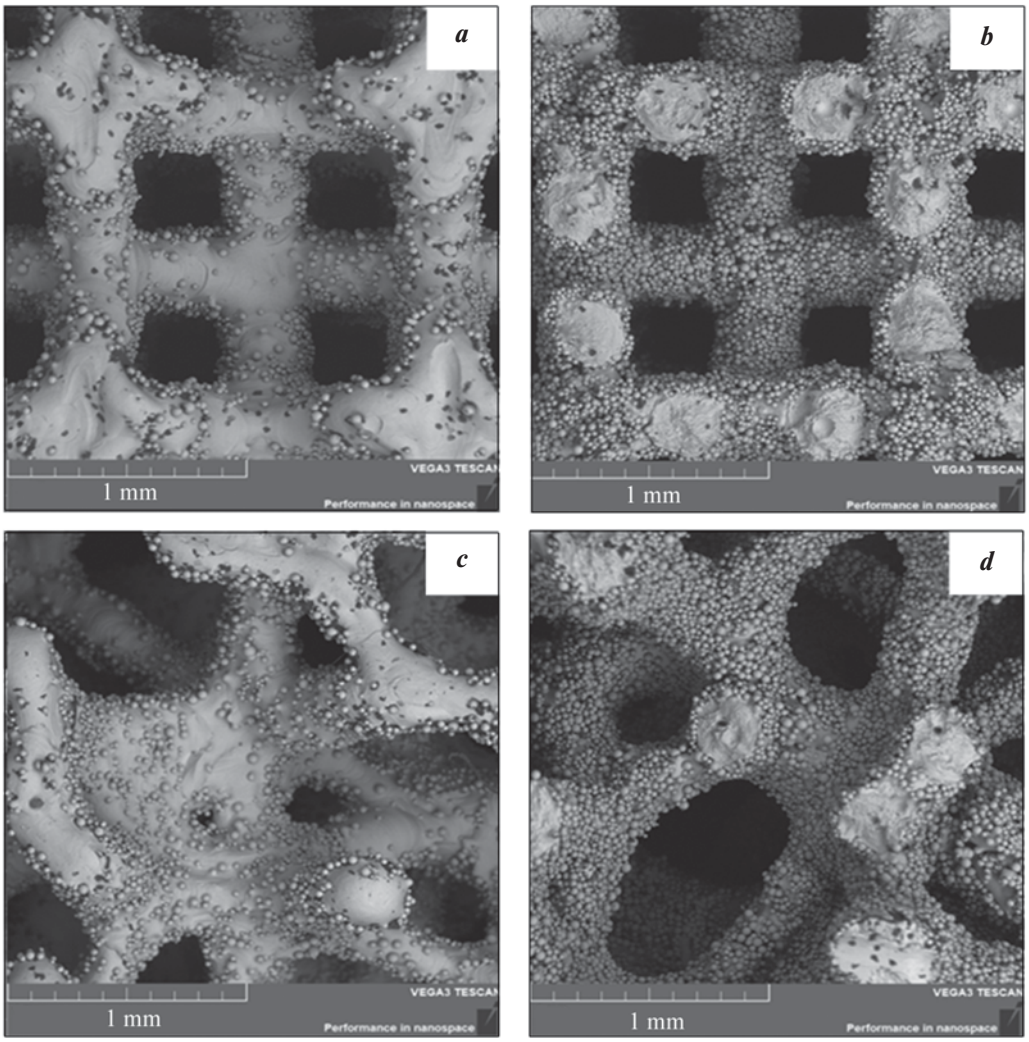


**Fig. 8.** Macrostructure of samples of porous structures of *D* type (***a***, ***b***) and *V* type (***c***, ***d***), obtained by regime *1*
***a***, ***c*** – top view, ***b***, ***d*** – bottom view

**Рис. 8.** Макроструктура образцов пористых структур типа *Д* (***a***, ***b***) и *В* (***c***, ***d***), полученных по режиму *1*
***a***, ***c*** – вид сверху, ***b***, ***d*** – снизу

according to mode *1*, it is 3 times lower than for samples made according to the manufacturer's mode, and is about 0.6 % (see Fig. 9, *e*).

The thickness of the struts of the *D* type structure, measured from microphotographs, is 265±15 μm and 245±14 μm for modes *1* and *T*. Any differences in the values of defect porosity and the average size of the struts are reflected in the total porosity of the samples: $p$ = 72.3±1.2 % for mode *T* and $p$ = 70.0±1.0 % for regime *1*.

Fig. 10 shows diagrams of deformation by compression of samples of porous structures of *D* and *V* types, fabricated in two regimes. Ultimate strength ($\sigma_u$) was determined from the point of the first sharp decrease in stress, corresponding to the primary destruction of one of the rows of struts of the porous structure.

A comparison of the mechanical properties of porous structures shows that the application of the regime developed leads to a significant increase in strength characteristics: increase in the yield strength from 76 to 132 MPa for *D* and from 66 to 86 MPa for *V* (see Fig. 10 and Table 4). A difference in the strength of the two types of structures is associated with a more optimal *D* design [5]. It should be noted that the Young's modulus changes slightly with a sufficiently significant increase in strength and remains in the range of 1—2 GPa. This corresponds to this indicator for spongy bone tissue. When comparing the

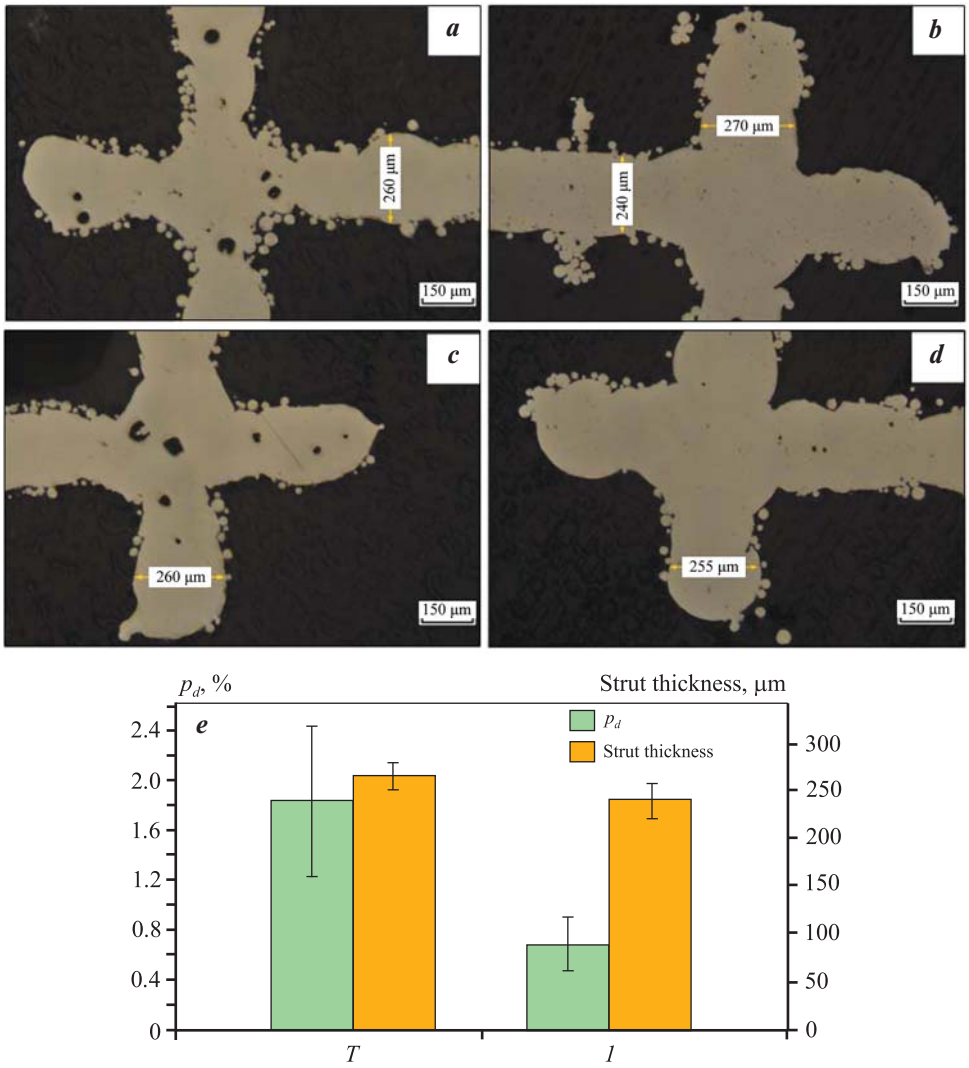


**Fig. 9.** Typical images of struts in samples of porous structures of *D* type obtained by regimes *T* (***a***, ***c***) and *1* (***b***, ***d***), ***e*** – the average size of the struts of samples of type *D* built according to different modes

**Рис. 9.** Типичные изображения перемычек в образцах пористых структур типа *Д*, полученных по режимам *T* (***a***, ***c***) и *1* (***b***, ***d***), ***e*** – средний размер перемычки образцов типа *Д* построенных по разным режимам

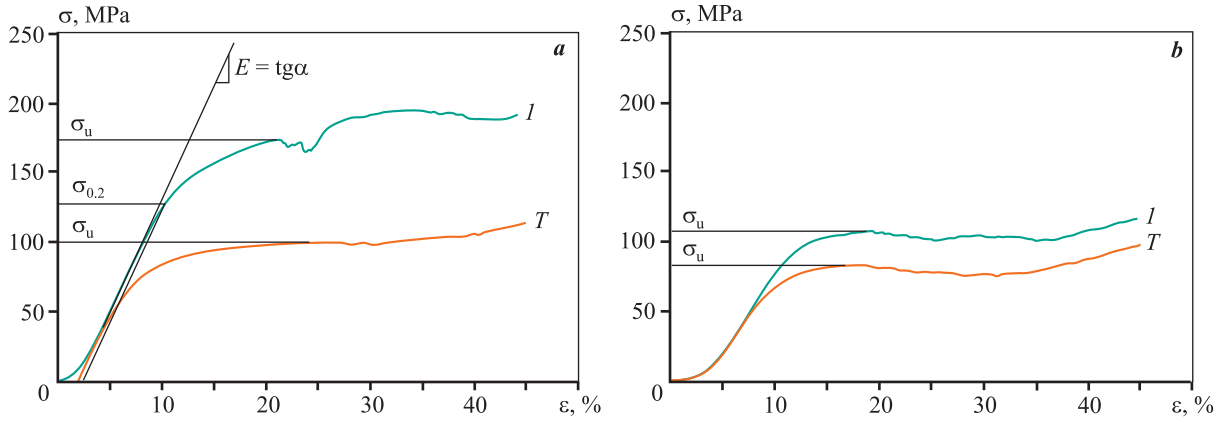


**Fig. 10.** Compression strain diagrams of samples of porous structures of *D* type (***a***) and *V* type (***b***), obtained by regimes *T* and *1*

**Рис. 10.** Диаграммы деформации сжатием образцов пористых структур типа *Д* (***a***) и *B* (***b***), полученных по режимам *T* и *1*

Table 4. **Mechanical properties of porous structures obtained by regimes *T* and *1* in comparison with analogues and types of bone tissue**

Таблица 4. Механические свойства пористых структур, полученных по режимам *T* и *1*, в сравнении с аналогами из литературы и типами костной ткани

| Structure type (SLM regime) | *p*, % | $\sigma_{0.2}$, MPa | $\sigma_u$, MPa | *E*, GPa |
|---|---|---|---|---|
| *D* (*P*) | 72.3±1.2 | 76±3 | 103±6 | 1.24±0.08 |
| *V* (*P*) | 74.5±1.5 | 66±4 | 80±4 | 1.09±0.14 |
| *D* (*1*) | 70.0±1.0 | 132±8 | 173±5 | 1.55±0.12 |
| *V* (*1*) | 73.4±1.3 | 86±6 | 104±5 | 1.25±0.10 |
| *V* [19] | 68.1±2.7 | 80±5 | 93±3 | 1.82±0.15 |
| *D* [12] | 70* | 140±6 | 174±4 | 4.89±0.05 |
| Bone tissue [11]: | | | | |
| cortical bone | – | 42–176 | – | 7–30 |
| trabecular bone | 40–80 | 0.2–10.5 | – | 0.04–2.0 |
| vertebrae | – | 3–6 | – | 0.37 |

* Porosity according to CAD model.

mechanical properties of the porous structures of two types build according to the developed SLM regime, the values of Young's modulus are lower than those of analogues with the same porosity and a comparable level of strength, (1.55±0.12 vs. 4.89 ±0.05 for *D* and 1.25±0.10 vs. 1.82±0.15 for *V*).

## Conclusions

Based on the results of the study of the influence of selective laser melting parameters on defect porosity, phase composition, microstructure and hardness of Ti—6Al—4V alloy, an approach to the improvement of SLM regimes in the production of highly porous materials with thin internal structural elements was developed. The method was efficiently applied in the manufacturing of porous structures of *D* and *V* type with a porosity of about 75 % developed for bone implants.

A decrease in the level of defect porosity from ≈1.8 to 0.6 %, provided by the use of the developed SLM regime, contributes to a significant increase in the strength characteristics of the material. This is seen in the increase in the yield stress of rhombic dodecahedron from 76 to 132 MPa and that of Voronoi polyhedron from 66 to 86 MPa. At the same time, a low Young's modulus (1—2 GPa) is maintained, corresponding to the level of stiffness of the spongy bone tissue.

## References

1. Shunyu Liu, Yung C. Shin, Additive manufacturing of Ti6Al4V alloy: A review. *Materials & Design*. 2019; 164:107552. https://doi.org/10.1016/j.matdes.2018.107552
2. Chlebus E., Kuźnicka B., Kurzynowski T., Dybała B. Microstructure and mechanical behaviour of Ti—6Al—7Nb alloy produced by selective laser melting. *Materials Characterization*. 2011;62(5):488—495. https://doi.org/10.1016/j.matchar.2011.03.006
3. Jalali M., Mohammadi K., Movahhedy M.R., Karimi F., Sadrnezhaad S.K., Chernyshikhin S.V., Shishkovsky I.V. SLM additive manufacturing of NITI porous implants: A review of constitutive models, finite element simulations, manufacturing, heat treatment, mechanical, and biomedical studies. *Metals and Materials International*. 2023. https://doi.org/10.1007/s12540-023-01401-1
4. Brailovski V., Kalinicheva V., Letenneur M., Lukashevich K., Sheremetyev V., Prokoshkin S. Control of density and grain structure of a laser powder bed-fused superelastic Ti—18Zr—14Nb alloy: Simulation-driven process mapping. *Metals*. 2020;10(12):1697. https://doi.org/10.3390/met10121697
5. Chen H., Han Q., Wang C., Liu Y., Chen B., Wang J. Porous scaffold design for additive manufacturing in ortho-

pedics: A review. *Frontiers in Bioengineering and Biotechnology*. 2020;8.
https://doi.org/10.3389/fbioe.2020.00609

6. Nune K.C., Misra R.D., Li S.J., Hao Y.L., Yang R. Cellular response of osteoblasts to low modulus Ti—24Nb—4Zr—8Sn alloy mesh structure. *Journal of Biomedical Materials Research. Pt. A*. 2016;105(3):859—870.
https://doi.org/10.1002/jbm.a.35963
7. Warnke P.H., Douglas T., Wollny P., Sherry E., Steiner M., Galonska S., Becker S.T., Springer I.N., Wilftang J., Sivenanthan S. Rapid prototyping: Porous titanium alloy scaffolds produced by selective laser melting for bone tissue engineering. *Tissue Engineering. Pt. C: Methods*. 2009;15(2):115—124.
https://doi.org/10.1089/ten.tec.2008.0288
8. Barba D., Alabort E., Reed R.C. Synthetic bone: Design by additive manufacturing. *Acta Biomaterialia*. 2019; 97:637—656.
https://doi.org/10.1016/j.actbio.2019.07.049
9. Yan C., Hao L., Hussein A., Young P. Ti—6Al—4V triply periodic minimal surface structures for bone implants fabricated via selective laser melting. *Journal of the Mechanical Behavior of Biomedical Materials*. 2015; 51:61—73.
https://doi.org/10.1016/j.jmbbm.2015.06.024
10. Taniguchi N., Fujibayashi S., Takemoto M., Sasaki K., Otsuki B., Nakamura T., Matsushita T., Kokubo T., Matsuda S. Effect of pore size on bone ingrowth into porous titanium implants fabricated by additive manufacturing: An in vivo experiment. *Materials Science and Engineering: C*. 2016;59:690—701.
https://doi.org/10.1016/j.msec.2015.10.069
11. Timercan A., Sheremetyev V., Brailovski V. Mechanical properties and fluid permeability of gyroid and diamond lattice structures for intervertebral devices: Functional requirements and comparative analysis. *Science and Technology of Advanced Materials*. 2021; 22(1):285—300.
https://doi.org/10.1080/14686996.2021.1907222
12. Li J., Chen D., Zhang Y., Yao Y., Mo Z., Wang L., Fan Y. Diagonal-symmetrical and midline-symmetrical unit cells with same porosity for bone implant: Mechanical properties evaluation. *Journal of Bionic Engineering*. 2019;16(3):468—479.
https://doi.org/10.1007/s42235-019-0038-z
13. Fantini M., Curto M.. Interactive design and manufacturing of a Voronoi-based biomimetic bone scaffold for morphological characterization. *International Journal on Interactive Design and Manufacturing (IJIDeM)*. 2017;12(2):585—596.
https://doi.org/10.1007/s12008-017-0416-x
14. Liu T., Guessasma S., Zhu J., Zhang W. Designing cellular structures for additive manufacturing using Voronoi—Monte Carlo approach. *Polymers*. 2019;11(7):1158.
https://doi.org/10.3390/polym11071158
15. Bhandari L., Gaur V. A study on defect-induced fatigue failures in SLM Ti6Al4V alloy. *Procedia Structural Integrity*. 2022;42:529—536.
https://doi.org/10.1016/j.prostr.2022.12.067
16. Sombatmai A., Uthaisangsuk V., Wongwises S., Promoppatum P. Multiscale investigation of the influence of geometrical imperfections, porosity, and size-dependent features on mechanical behavior of additively manufactured Ti—6Al—4V lattice struts. *Materials & Design*. 2021;209:109985.
https://doi.org/10.1016/j.matdes.2021.109985
17. Letenneur M., Kreitcberg A., Brailovski V. Optimization of laser powder bed fusion processing using a combination of melt pool modeling and design of experiment approaches: Density control. *Journal of Manufacturing and Materials Processing*. 2019;3(1):21.
https://doi.org/10.3390/jmmp3010021
18. Saremian R., Badrossamay M., Foroozmehr E., Kadkhodaei M., Forooghi F. Experimental and numerical investigation on lattice structures fabricated by selective laser melting process under quasi-static and dynamic loadings. *The International Journal of Advanced Manufacturing Technology*. 2021;112(9-10):2815—2836.
https://doi.org/10.1007/s00170-020-06112-0
19. Zhu L., Liang H., Lv F., Xie D., Wang C., Mao Y., Yang Y., Tian Z., Shen L. Design and compressive fatigue properties of irregular porous scaffolds for orthopedics fabricated using selective laser melting. *ACS Biomaterials Science & Engineering*. 2021;7(4):1663—1672.
https://doi.org/10.1021/acsbiomaterials.0c01392
20. Jimenez E.H., Kreitcberg A., Moquin E., Brailovski V. Influence of post-processing conditions on the microstructure, static, and fatigue resistance of laser powder bed fused Ti—6Al—4V components. *Journal of Manufacturing and Materials Processing*. 2022;6:85.
https://doi.org/10.3390/jmmp6040085
21. Van Hooreweder B., Apers Y., Lietaert K., Kruth J.P. Improving the fatigue performance of porous metallic biomaterials produced by selective laser melting. *Acta Biomaterialia*. 2017;47:193—202.
https://doi.org/10.1016/j.actbio.2016.10.005

## Information about the authors

**Vadim A. Sheremetyev** – Cand. Sci. (Eng.), Leading Researcher, Metal Forming Department, National University of Science and Technology "MISIS" (NUST MISIS).
http://orcid.org/0000-0002-2086-0628
E-mail: vadim.sheremetyev@gmail.com

**Viacheslav D. Lezin** – Postgraduate, Research Laboratory Assistant, Metal Forming Department, NUST MISIS.
http://orcid.org/0000-0002-7568-2005
E-mail: vyacheslavlezin@gmail.com

**Marina V. Kozik** – Master Student, Research Laboratory Assistant, Metal Forming Department, NUST MISIS.
http://orcid.org/0009-0001-9857-973X
E-mail: marinakozik627@gmail.com

**Sergey A. Molchanov** – Head of Quality Service, LLC "Conmet".
http://orcid.org/0009-0001-7237-3872
E-mail: molchanov@conmet.ru

## Информация об авторах

**Вадим Алексеевич Шереметьев** – к.т.н., ведущий научный сотрудник кафедры обработки металлов давлением (ОМД), Национальный исследовательский технологический университет «МИСИС» (НИТУ МИСИС).
http://orcid.org/0000-0002-2086-0628
E-mail: vadim.sheremetyev@gmail.com

**Вячеслав Дмитриевич Лезин** – аспирант, лаборант-исследователь кафедры ОМД, НИТУ МИСИС.
http://orcid.org/0000-0002-7568-2005
E-mail: vyacheslavlezin@gmail.com

**Марина Владимировна Козик** – студент-магистр, лаборант-исследователь кафедры ОМД, НИТУ МИСИС.
http://orcid.org/0009-0001-9857-973X
E-mail: marinakozik627@gmail.com

**Сергей Алексеевич Молчанов** – начальник службы качества, ООО «Конмет».
http://orcid.org/0009-0001-7237-3872
E-mail: molchanov@conmet.ru

## Contribution of the authors

**V.A. Sheremetyev** – formulated the research objectives, conducted experiments, wrote and revised the manuscript.

**V.D. Lezin** – prepared materials and initial samples, prepared the manuscript.

**M.V. Kozik** – prepared polished samples and obtained micrographs, participated in the discussion of the results.

**S.A. Molchanov** – participated in the discussion of the results.

## Вклад авторов

**В.А. Шереметьев** – определение цели работы, проведение экспериментов, написание и корректировка текста статьи.

**В.Д. Лезин** – подготовка материалов и исходных образцов, подготовка текста статьи.

**М.В. Козик** – подготовка шлифов и получение микроснимков, участие в обсуждении результатов.

**С.А. Молчанов** – участие в обсуждении результатов.

*The article was submitted 24.04.2023, revised 28.04.2023, accepted for publication 03.05.2023*

*Статья поступила в редакцию 24.04.2023, доработана 28.04.2023, подписана в печать 03.05.2023*